Journal of Materials and Environmental Science
ISSN : 2028-2508
e-ISSN : 2737-890X
CODEN : JMESCN

J. Mater. Environ. Sci., 2026, Volume 17, Issue 2, Page 326-344

http://www.jmaterenvironsci.com

Synthesis and characterization of activated carbon from bean pods: adsorption kinetics of methylene blue dye, adsorption isotherms and intra-particle diffusion

Sodoadika Akpolou[1*], Samadou Sanni[2], Yahouza Zaneidou[3], Ibrahim Tchakala[2], Moursalou Koriko[1], Gado Tchangbedji[1]

[1]Laboratoire de Gestion, de Traitement et de Valorisation des Déchets, Université de Lomé (GTVD/UL), Lomé, Togo
[2]Laboratory of Applied Hydrolgy and Environment, University of Lome (LHAE/UL), Lomé, Togo
[3]Faculty of Education Sciences, Djibo Hamani University, P. B. 255 Tahoua, Tahoua, Niger

**Corresponding author, Email address: sodoadikaa@gmail.com*

Received *13 Jan 2026,*
Revised *14 Feb 2026,*
Accepted *16 Feb 2026*

Keywords:

- ✓ *Activated carbon;*
- ✓ *Bean pods;*
- ✓ *Methylene blue;*
- ✓ *Adsorption;*
- ✓ *Intra-particle diffusion*

Citation*: Akpolou S., Sanni S., Zaneidou Y., Tchakala I., Koriko M., Tchangbedji G. (2026) Synthesis and characterization of activated carbon from bean pods: adsorption kinetics of methylene blue dye, adsorption isotherms and intra-particle diffusion, J. Mater. Environ. Sci., 17(2), 326-344.*

Abstract: The dyes poses a threat to the aquatic organisms, human health and the environment. This study aims to prepare activated carbon bean pods (ABPC) from bean pods in Togo and apply it for the methylene blue (MB) dye adsorption. To this end, the phosphoric acid chemical method was adopted for the synthesis of activated carbon. Furthermore, physicochemical and textural characterizations were performed, including analyses by Fourier transform infrared (FTIR) spectroscopy, X-ray diffraction (XRD), scanning electron microscopy (SEM), energy-dispersive X-ray (EDX) spectroscopy, and the Lopez-Ramon method (1999). To evaluate the adsorption capacity of the activated carbon, an experimental study of MB dye removal using the batch method was conducted. First-order and second-order adsorption kinetics, Langmuir and Freundlich adsorption isotherms, and intraparticle diffusion were determined. Specifically, the mass yield and low ash content, parameters indicating the amorphous state of the adsorbent, and the pH at the zero-charge point (pH_{ZPC} = 5.16) were determined. FTIR spectroscopy analysis reveals the chemical bonds related to predominantly acidic functional groups, while XRD indicated the absence of crystallization in the activated charcoal. SEM at 100 µm illustrates the picture of the surface of the charcoal. EDX analysis of the activated charcoal reveals the presence of carbon and oxygen. Characterization and experimental results show that the ABPC is amorphous. Experimental adsorption studies reveal a MB removal rate exceeding 98%; Langmuir and Freundlich adsorption isotherms, the pseudo-first-order kinetic model, the second-order model, and intraparticle diffusion were investigated. ABPC is therefore a potential alternative adsorbent for wastewater treatment.

1. Introduction

The textile industry uses synthetic dyes to color various products such as fibers and yarns (Abdelhafez *et al.*, 2025). These synthetic dyes are non-biodegradable organic compounds with aromatic structures, known for their toxicity, mutagenic, and carcinogenic properties (Din *et al.*, 2024; Baari *et al.*, 2025). Wastewater generated by these industries is heavily laden with dyes. This industrial wastewater is often discharged into rivers, streams, lakes, and the environment. The presence of these dyes in surface waters poses a threat to the environment, human health, and aquatic

life. Methylene blue (MB), a dye with a stable aromatic structure, can cause gastrointestinal irritation, nausea or vomiting, dyspnea, and cyanosis if ingested (Ismail *et al.,* 2025). These dyes lead to reduced light penetration into waters, limiting photosynthesis, disrupting aquatic life and degrading water quality (Aljeboree *et al*., 2024; Abdelhafez *et al*., 2025).

Agricultural activities lead to the production of ever-increasing by-products. Whether cereals, legumes, or tubers, a portion of crops is discarded as waste after harvest. These agricultural residues are primarily composed of cellulose, hemicellulose, and lignin. Poor management and the proliferation of these residues in the biosphere contribute to the degradation of quality of life, surface water pollution, and environmental degradation. Transforming agri-food residues into activated carbon offers a sustainable, value-added product alternative; it contributes to promoting the circular economy and reducing environmental pollution (Alkhawaja & Abdul-Hameed, 2025; Kaga *et al*., 2024). Previous studies have addressed the production and uses of activated carbon. Furthermore, activated carbons are adsorbents that find applications in water treatment, gas purification, and dye removal (Balogoun *et al.* , 2015; Akartasse *et al.,* 2022; Faouzou *et al*., 2024). Various local agricultural residues have been used as precursor materials for activated carbons. For example, cotton residual (Tchakala *et al.,* 2012), corn cobs and stalks (Armand *et al*., 2020; Kumaravel *et al*., 2024), peanut shells (Diallo *et al*., 2022), Typha (N'diaye *et al*., 2022), and coconut shells (Saleem *et al*., 2025) have been used to prepare activated carbons using the chemical activation method. In reality, there are two activation modes: chemical activation (400°C–700°C) and physical activation (800°C–1000°C) (Shamsuddin *et al*., 2016). The two most commonly used chemical agents are zinc chloride and phosphoric acid. In recent years, phosphoric acid has been used more frequently in the chemical activation of coal, not only for economic and environmental reasons, but also because it contributes to the proliferation of micro- and mesoporosities in the coal matrix (Zayed *et al*., 2023). The applications of adsorbents depend on understanding their properties, which are in turn deduced from physicochemical and textural characterizations.

The common bean, *Phaseolus vulgaris,* is a legume cultivated for its protein-rich seeds in various regions of Togo. After harvesting and shelling, the bean pods, the elongated coverings containing the seeds, are discarded; they are part of the agricultural residues generated and left behind after harvest. However, they can be used to produce value-added products, such as activated carbon.

The most widespread method for treating bean by-products remains combustion, which generates harmful gases, contributing to environmental pollution. The preparation of activated carbon requires an economic investment that impacts its uses, even though it is effective for water treatment (Atheba *et al*., 2014). It is necessary to find simple, local resources to ensure the production of adsorbents at a lower cost. Bean husks, available locally, are a biomass that can be transformed into activated carbon, as an alternative to commercial activated carbon. Therefore, precursor materials, bean husks, were collected from farmers in the Maritime Region of Togo for processing into activated carbon.

The objective of this study is to prepare activated carbon from bean pods and to characterize it using physicochemical and textural methods. Furthermore, the study aims to apply the carbon to the removal of methylene blue dye. The activated carbon is prepared using a chemical activation method with phosphoric acid. Characterization techniques include X-ray diffraction (XRD), Fourier transform infrared spectroscopy (FTIR), scanning electron microscopy (SEM) coupled with energy-dispersive X-ray spectroscopy (EDX), the Lopez-Ramon method, and ash content determination.

First-order and second-order adsorption kinetics, Langmuir and Freundlich adsorption isotherms, and intra-particle diffusion were determined.

2. Materials and methods

2.1 Materials and chemicals

The raw materials used for the synthesis of activated carbon are bean pods (*Phaseolus vulgaris*). These precursor materials, bean pods, were collected from farmers at the Maritime Region of Togo. To prepare the activated carbon and perform the physicochemical analyses, the following chemical reagents were used.

Phosphoric acid H_3PO_4 (85%) is purchased from Park Scientific Limited, Northampton, UK; hydrochloric acid (ACS, 37%) is from Merk KGaA, Darmstadt Germany, USA; sodium chloride (NaCl $\geq$ 99.5%), sodium hydroxide (NaOH, 98%), methylene blue (Molecular mass: 319.85 $g \cdot mol^{-1}$, chemical formula : $C_{16}H_{18}N_3SCl$) are purchased from Sigma Aldrich, St Louis, MO, USA.

2.2 Preparation of activated charcoal

The sample was then washed with distilled water to remove impurities and dried at room temperature on a laboratory bench. Using a blender, the pods were ground into small pieces and then dried again, this time in an oven (ISUZU brand) at 105°C for 24 hours before impregnation.

After drying, the pods were impregnated with a dilute H_3PO_4 50% phosphoric acid solution at a ratio of 2 (2g of phosphoric acid to 1g of precursor). The resulting mixture was thoroughly kneaded using a stick. The impregnated solution was then stored in a sealed container for 24 hours to allow for carbonization. The impregnate is distributed into pre-dried porcelain crucibles; these are weighed and placed in a container, a metal jar designed and adapted to hold the sample crucibles. The jar containing the samples is placed in the electric furnace (SNOL brand). Carbonization is a pyrolysis process carried out at 400°C for 2 hours. The temperature rises from ambient to 400°C, where it stabilizes within a range for 2 hours before decreasing. The carbonized material, activated carbon, is removed from the furnace, placed in a desiccator for cooling, and then weighed before washing. The mass yield of production and the activation rate (burn-off) of activated carbon are determined by **Eqn. 1** and **Eqn. 2**:

$$\text{Mass}\ (\%) = \frac{m_{AC}}{m_{Precursor}} \times 100 \qquad \textbf{Eqn. 1}$$

$$\text{Burn-Off}(\%) = \frac{(m_{Precursor} - m_{AC})}{m_{Precursor}} \times 100 \qquad \textbf{Eqn. 2}$$

The activated carbon is washed first in a hydrochloric acid solution (0.1M) for 24 hours, then thoroughly washed with distilled water until the residual water reaches a constant pH (pH200E meter). After filtration and drying at 105°C for 24 hours, the activated carbon is stored in a sealed container for characterization.

2.3 Characterization

The activated carbon produced is characterized using physico-chemical and textural analysis techniques, including X-ray diffraction (XRD), Fourier transform infrared spectroscopy (FTIR), scanning electron microscopy (SEM) coupled with energy-dispersive X-ray (EDX) analysis,

thermogravimetric analysis, the Lopez-Ramon method (1999), and the ash content determination method.

X-ray diffraction (XRD) techniques performed at angles 2θ ranging from 5° to 69.8° using a Brucker D8 Advance diffractometer equipped with a copper anode and the ash content determination technique (Armand *et al.*, 2020) were used to identify the mineralogical composition and crystalline phases present in the coal. Scanning electron microscopy (SEM) coupled with energy-dispersive X-ray spectroscopy (EDX) enabled observation of the pore distribution on the surface of the activated carbon and its elemental chemical composition. Fourier transform infrared (FTIR) spectroscopy was used to study the surface chemistry by identifying chemical functional groups. Thermogravimetric analyses (TGA) were performed to investigate the thermal stability of the prepared activated carbon and to determine the different decomposition phases. The Lopez-Ramon method (1999) (Tchakala *et al.*, 2012)was used to determine the pH at the zero-charge point, and the burn-off value was determined to infer the nature of the material's porosity.

Knowledge of these characteristics will not only allow us to evaluate the adsorption capacity of the analyzed activated carbon, but will also guide its application in the context of pollutant removal.

2.4 Experimental study of activated carbon adsorption

To determine the usefulness of activated bean pods carbon (ABPC), as an adsorbent, the adsorption of a model dye, methylene blue (MB), was studied. First, $1\,g\cdot L^{-1}$ of MB stock solution was prepared by dissolving 1 g of MB powder in a 1000 mL volumetric flask with distilled water. Several daughter solutions were prepared by diluting an appropriate volume of the stock solution, and then calibration was performed. The absorbance of the solutions were read using a Ultraviolet-visible (UV-vis) spectrophotometer (INESA 754N) at a wavelength of $\lambda = 620$ nm. The equation used to calculate the residual concentrations of the MB solutions was determined by plotting the absorbance versus MB concentrations ($mg\cdot L^{-1}$) line by Origin.

Experimental studies of MB adsorption on ABPC were conducted by applying a batch method. A quantity of ABPC was introduced into a 250 mL beaker containing 200 mL of a MB solution of a given initial concentration. The mixture (ABPC + MB) was then subjected to magnetic stirring (using SCIENTIFIC brand stirrer) at 300 rpm. At regular intervals, samples were taken, the residual concentrations of MB were determined. Furthermore, the effect of ABPC mass and the effect of initial concentrations on the equilibrium time adsorption were investigated. The initial concentrations of MB solutions values such as $20\,mg\cdot L^{-1}$, $30\,mg\cdot L^{-1}$, $40\,mg\cdot L^{-1}$, $50\,mg\cdot L^{-1}$ were used to carry out the adsorption experiment on 0.1g, 0.2g and 0.3g of ABPC.

The amount of MB adsorbed per unit mass and the percentage of ABPC elimination are determined by using the equations **Eqn. 3** and **Eqn. 4**:

$$q(mg\cdot g^{-1}) = \frac{(C_0 - C_e)V}{m} \qquad \textbf{Eqn. 3}$$

$$\text{Removal}(\%) = \frac{(C_0 - C_e)}{C_0}\times 100 \qquad \textbf{Eqn. 4}$$

C_0 and C_e denote the initial concentration of MB and the equilibrium concentration of BM, respectively; m and V represent the mass of ABPC and the adsorption volume, respectively. First-order and second-order kinetic adsorption studies, Langmuir and Freundlich adsorption isotherms,

and intraparticle diffusion were explored to explain the interactions between MB molecules and ABPC.

2.4.1 Kinetic and isothermal studies of adsorption

2.4.1.1 Adsorption Isotherms

Adsorption isotherms relate, at a given temperature, the quantities of adsorbate molecules to the quantities of adsorbents at equilibrium. They analyze experimental data and facilitate the description of pollutant adsorption. The Langmuir and Freundlich models were applied to analyze experimental data of the adsorbent-pollutant system. The Langmuir adsorption isotherm is obtained by plotting the graph of $(\frac{1}{q_e})$ versus $(\frac{1}{C_e})$ while the Freundlich adsorption isotherm is obtained from the plot of $\ln(q_e)$ versus $\ln(C_e)$. **Eqn. 5** and **Eqn. 6** represent Langmuir and Freundlich isotherms respectively (Abdelhafez *et al*., 2025; Bortoluz *et al*., 2020; Din *et al*., 2024).

$$\frac{1}{q_e} = \frac{1}{q_{max} K_L} \frac{1}{C_e} + \frac{1}{q_{max}} \qquad \textbf{Eqn. 5}$$

$$\ln(q_e) = \ln(K_f) + \frac{1}{n} \ln(C_e) \qquad \textbf{Eqn. 6}$$

$K_L\,(mg \cdot L^{-1})$ and $q_{max}\,(mg \cdot g^{-1})$ respectively denote the Langmuir constant and the maximum adsorption capacity; K_L characterizes the interactions between the BM dye and the CAH; characterizes the strength of an adsorption. The parameters $q_{max}, K_L, R_L, \frac{1}{n}$, K_f are determined by **Eqn. 7**, **Eqn. 8**, **Eqn. 9**, **Eqn. 10**, and **Eqn. 11**.

$$q_{max} = \frac{1}{\text{Intercept}} \qquad \textbf{Eqn. 7}$$

$$K_L = \frac{1}{\text{Slope} \cdot q_{max}} \qquad \textbf{Eqn. 8}$$

$$R_L = \frac{1}{1 + C_i \cdot K_L} \qquad \textbf{Eqn. 9}$$

$$\frac{1}{n} = \text{Slope} \qquad \textbf{Eqn. 10}$$

$$K_f = \text{Antiln(Intercept)} \qquad \textbf{Eqn. 11}$$

K_f and $\frac{1}{n}$ are Freundlich constants; K_f determines the adsorption capacity and $\frac{1}{n}$ measures the heterogeneity of the adsorption intensity or the degree of non-linearity (Baari *et al*., 2025).

2.4.1.2 Adsorption kinetics

Adsorption kinetics according to two kinetic models, pseudo-first order and pseudo-second order, were analyzed. The adsorption kinetics of the pseudo-first order and the adsorption kinetics of the pseudo-second order are obtained by plotting the graph of ln $\ln(q_e - q_t)$ versus time (t) and the graph of $\frac{t}{q_t}$ versus t (time), represented by **Eqn. 12** and **Eqn. 13** respectively:

$$\ln(q_e - q_t) = \ln(q_e) - k_1 \cdot t \qquad \textbf{Eqn. 12}$$

$$\frac{t}{q_t} = \frac{1}{k_2 \cdot q_e^2} + \frac{1}{q_e} \cdot t \qquad \textbf{Eqn. 13}$$

The rate constants k_1 and k_2 the amount MB adsorbed at equilibrium are determined from the equations of the linear fit lines corresponding to equations **Eqn. 12** and **Eqn. 13**

Pseudo-first-order kinetics assumes that the reaction rate is proportional to the concentrations of dyes/pollutants in the solution and is controlled by surface interactions of the adsorbent. However, pseudo-second-order kinetics assumes that adsorption is chemical in nature and occurs in determinate steps; it allows us to deduce whether there are interactions between the adsorbate molecules and the adsorbent surface, interactions which will potentially enhance adsorption.

2.4.2 Intra-particle diffusion

The adsorption of dyes can be explained by the intra-particle diffusion model. When adsorption reactions occur via intra-particle diffusion, the curve representing the quantity of dye adsorbed per unit mass of adsorbent (q_t) versus square root of time ($t^{\frac{1}{2}}$) is a straight line, represented by **Eqn. 14**

$$q_t = k_d \cdot t^{\frac{1}{2}} + C \qquad \textbf{Eqn. 14}$$

k_d is the intraparticle diffusion constant and C ($mg \cdot g^{-1}$) is the constant that characterizes the boundary layer thickness. When the value of the constant C is zero, intraparticle diffusion is the limiting phenomenon of the adsorption process; when it is negative, adsorption is slow; it is fast when C is positive (Bassareh *et al*., 2023).

3. Results and discussion

3.1 Mass yield and activation rate

The mass yield of activated carbon from bean pods is 44.32%, and the corresponding activation rate is 55.68%. This high activation rate, or loss on ignition (greater than 50%), indicates that the activated carbon will tend to develop medium to large pores (mesopores and macropores). Loss on ignition (burn-off) is due to the loss of volatile matter and particles under the effect of heat during carbonization, ultimately creating pores within the material (Tchakala *et al*., 2012). The nature of the pores depends on the precursor materials, as well as the preparation conditions.

3.2 The ash content

The mineral content of activated carbon is assessed based on the ash content. The ash content of the activated carbon was determined using the standard method. The activated carbon produced has an ash content of 2.51%. This relatively low value indicates that activated carbon prepared from bean pods is an amorphous porous solid composed primarily of carbon. Similar results have been reported in the literature for activated carbon made from cashew nut shells at 400°C (5.66%) (Brou Guillaume *et al*., 2019) and activated carbon prepared from the kernel shell of *Balanites aegyptiaca* (6.66%) (Maazou *et al*., 2018). Indeed, the high ash content of activated carbons reduces their pollutant

adsorption capacity; the minerals constituting the ash obstruct certain pores (Mamane *et al*., 2018; Ouedrhiri *et al*., 2018) and prevent access to adsorption sites.

3.3 The pH at the point of zero charge of activated carbon

The pH at the point of zero charge (pH_{ZPC}) of activated carbon analyzed by the bisector method, is shown in **Figure 1.a** and is equal to 5.16. This value, less than 7, is correlated with the acidic functional groups (lactones, carbonyls, carboxyls) present on the surface of the produced charcoal. This may be due to the raw material and the phosphoric acid chemical activation method used during charcoal preparation. Similar results have been reported in some studies in the literature, particularly for activated charcoals obtained by phosphoric acid activation of the kernel shells of *Balanites aegyptiaca (L.) Del. fruits* (pH_{ZPC} = 5.08) (Mamane *et al*., 2018), cottonseed cake (pH_{ZPC} = 5.3) (Tchakala *et al*., 2012), and corn cobs (pH_{ZPC} = 5.3) (Armand *et al*., 2020). The value of pH at the point of zero charge contributes to predicting the adsorption mechanism of pollutants in aqueous solution and helps to explain the optimal conditions for cationic or anionic adsorption (Asuquo *et al*., 2017). At the point of zero charge, the surface of the carbon carries as many negative charges as positive charges, which neutralize each other. Adsorbents with high values of pH_{ZPC} have a greater affinity for adsorbing anionic pollutants, while those with low values are more favorable for binding cationic pollutants (Usman *et al*., 2025). If the pH is low ($pH < pH_{ZPC}$), there is protonation of the oxygenated sites on the carbon surface, which becomes positively charged, leading to cation repulsion. Thus, the adsorption capacity of the adsorbent for cationic pollutants under this condition is reduced. However, when the pH is high ($pH > pH_{ZPC}$), the surface of the adsorbent becomes negatively charged, which is favorable to the adsorption of cations from pollutants through electrical attraction (Yunusa, Umar *et al*., 2020).

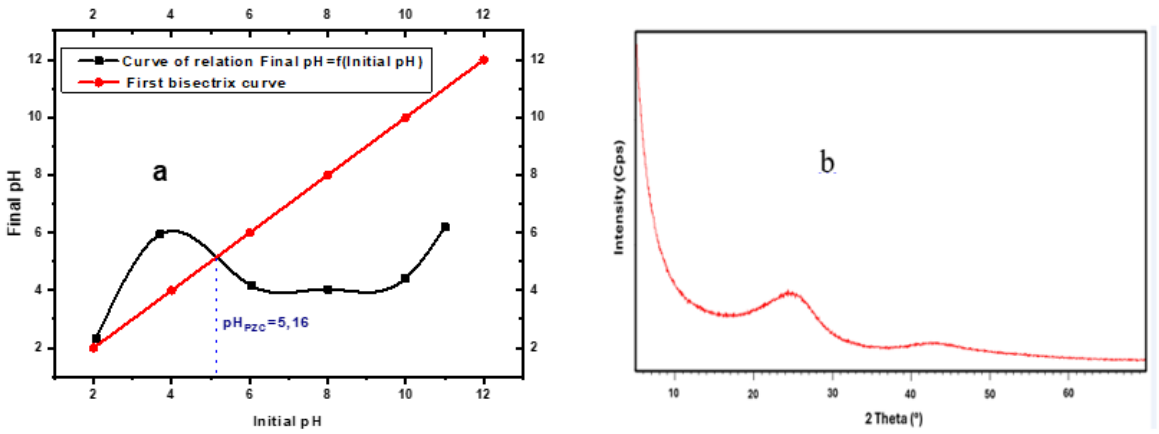

Figure 1. pH at the point of zero charge (a), X-rays diffraction (XRD) (b)

3.4 X-ray diffraction analysis (XRD)

The curve representing the results of the X-ray diffractometer analysis of activated bean pods is shown in **Figure 1.b**. This curve illustrates the structure of the sample exposed to X-rays, which characterizes the arrangement of atoms that constitute the sample matrix. Analysis of the diffractometer reveals two broad peaks around 25° and 43° for 2θ, characteristic of an amorphous structure present in the pod matrix (Suyoga Wiguna *et al*., 2024; Touzani *et al*., 2024). The activated bean pods are therefore an amorphous solid and contain no crystalline structure (Collins Ngoe *et al*.,

2018). This is similar to XRD analysis results from previous work on activated carbons prepared from plant precursors, showing the absence of crystallization (Kifuani Kia Mayeko *et al* ., 2012; Shamsuddin *et al* ., 2016; Zięzio *et al* ., 2020). However, a difference is noted when comparing with the XRD analysis results of activated charcoal prepared from corn cobs by chemical activation with phosphoric acid, which has a crystalline structure (Farma, 2019 ; Olorundare *et al* ., 2014) .

3.5 Fourier transform Infrared (FTIR) spectroscopy

Fourier transform infrared spectroscopy (FTIR) was performed to identify the functional groups present on the surface of the activated carbon and the raw material. For this purpose, infrared spectroscopy, carried out in a wavenumber range of 500 cm^{-1} to 4500 cm^{-1}, revealed peaks or absorption bands characteristic of the functional groups. The infrared spectrum of the analyzed activated carbon and raw material is shown in **Figure 2**. The main chemical bonds and their absorption numbers are listed in **Table 1**. The absorption spectrum of activated carbon and the material shows prominent bands with absorption peaks. The absorption band centered on 3655 cm^{-1} is attributed to hydroxyl group (-OH) stretching vibrations (Ojstršek *et al*., 2022) (Mahmoud *et al*., 2025)of alcohols (Al-Asadi *et al*., 2025), phenols, and carboxylic acids. The intense absorption peaks corresponding to wavenumbers 2956 cm^{-1}, 2914 cm^{-1}, 2877 cm^{-1}, 2836 cm^{-1} are due to the stretching vibrations of the CH bonds (Allahkarami *et al*., 2023) (CH_2) and methyl (CH_3) groups. (Salama *et al*., 2024; Sanni *et al*., 2025). The appearance of low-intensity peaks in the CAH spectrum at 2173 cm^{-1} and 2034 cm^{-1} is associated with C=N bond vibrations (Salama *et al*., 2024) or C≡C bond vibrations of alkynes (Aljeboree *et al*., 2014); while the peak appearing at 1739 cm^{-1} is due to C=O bond vibrations (Ojstršek & Gorgieva, 2024) of aldehyde groups, saturated carboxylic acids or acetyl groups in hemicelluloses (Shamsuddin *et al*., 2016). These low-intensity vibrations observed are associated with the aromatization and formation of oxygen groups (aldehyde, ketone, ester, carboxylic acid) that occurred during phosphoric acid activation and calcination at 400°C.

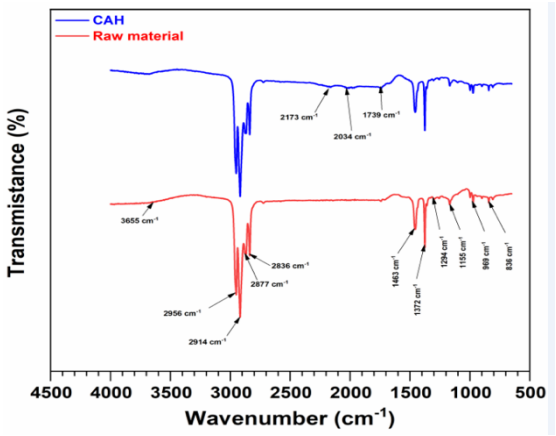

Figure 2. Fourier Transform Infrared (FTIR) spectra of ABPC and raw material

The peak observed at 1155 cm^{-1} can be attributed to the stretching vibrations of O-P-O (Al Lafi & Khuder, 2025), P-O-C, P=O, P=OOH (Zayed *et al*., 2023), characteristic of phosphates or polyphosphates (Alouiz et *al*., 2025), while the peak identified at 1294 cm^{-1} corresponds to the presence of phenol and lactone groups (Kanawade & Gaikwad, 2011) or to the N-H bond characteristic of amides III (Lv *et al*., 2024). Peaks 1453 cm^{-1} and 1372 cm^{-1} originate respectively

from the vibrations of the C=C, C-C bonds of aromatic groups (Dunston *et al*., 2025; Fitri Faradilla *et al*., 2021) and the vibrations of the OH groups of phenols (Raheel *et al.*, 2024), or from the angular deformation of the C-H groups of hemicelluloses (Bortoluz *et al*., 2020). In addition, the peaks identified around 969 cm^{-1} and 836 cm^{-1} are attributed to the out-of-plane bending of the C-H bonds (Dunston *et al*., 2025) attached to aromatic rings or alkene groups (Sudarsan *et al.,* 2025). Furthermore, the presence of functional groups (lactones, carbonyl, carboxyl) indicates that the surface of activated carbon contains predominantly acidic chemical functions (Khadiran *et al*., 2014) (Fathy *et al.*, 2012). This is consistent with the pH value at the zero charge point charge (pH_{ZPC} = 5.16). The presence of oxygenated groups (aldehydes, ketones, lactones, carboxylic acids, carbonyls, esters) on the surface of the activated carbon justifies the lignocellulosic nature of the precursors, bean pods (Balogoun *et al.*, 2015). Furthermore, the presence of carboxyl acid, ketone, and phenol groups makes ABPC a potential adsorbent of cationic pollutants (Saleem, 2024).

3.6 Scanning electron microscopy coupled with energy-dispersive X-rays (SEM/EDX)

The **Figure 3** shows the image of the observation by the SEM at 100 µm and the EDX micrograph of the ABPC, while **Figure 4** highlights the main constituent chemical elements of ABPC by energy-dispersive X-ray (EDX) analysis. Scanning electron microscopy observations at 100 µm illustrate the diverse porosity developed on the surface of the ABPC; in addition to the pores, particles are present on the surface of the activated carbon. The particles revealed are residues that occurred during the carbonization of plant-based precursors (Hazourli & Ziati, 2007). Pore formation depends on the activating agent used and the carbonization process. Indeed, phosphoric acid molecules integrate into the biomass, modifying its structure by forming bonds with atoms during impregnation.

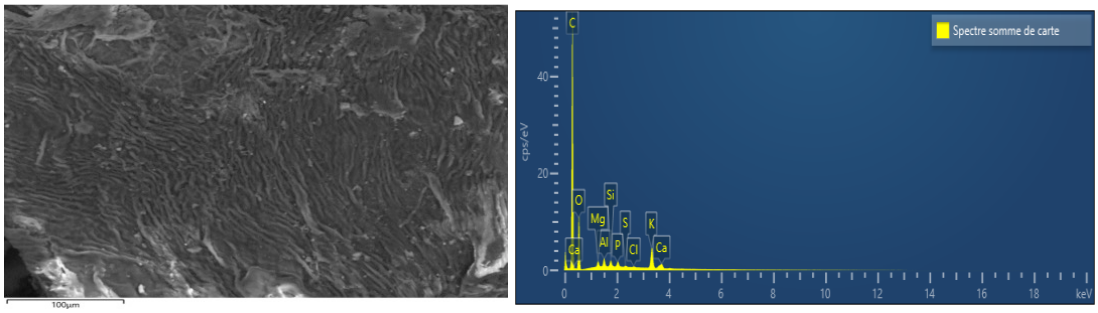

Figure 3. SEM/EDX image of ABPC

During carbonization, these bonds between atoms and the activating agent molecules, phosphoric acid, break. Under the effect of heat, these activating agent molecules, as well as other chemical species, escape from the material as a gaseous mixture, subsequently leaving voids or pores (Fathy *et al.*, 2012; Olorundare *et al*., 2014). Evaporation H_3PO_4 during carbonization promotes porosity development and explains the porous nature of activated carbon (Zayed *et al*., 2023). Furthermore, carbons with small accessible pores have a better adsorption capacity than adsorbents with large pores (Atheba *et al*., 2014). The elemental chemical composition of ABPC, determined by energy-dispersive X-ray (EDX) spectroscopy, is shown in **Table 2**. Each identified chemical element is accompanied by its atomic percentage. Analysis of these elemental chemical composition results indicates that activated carbon has a high carbon content (77.83%).

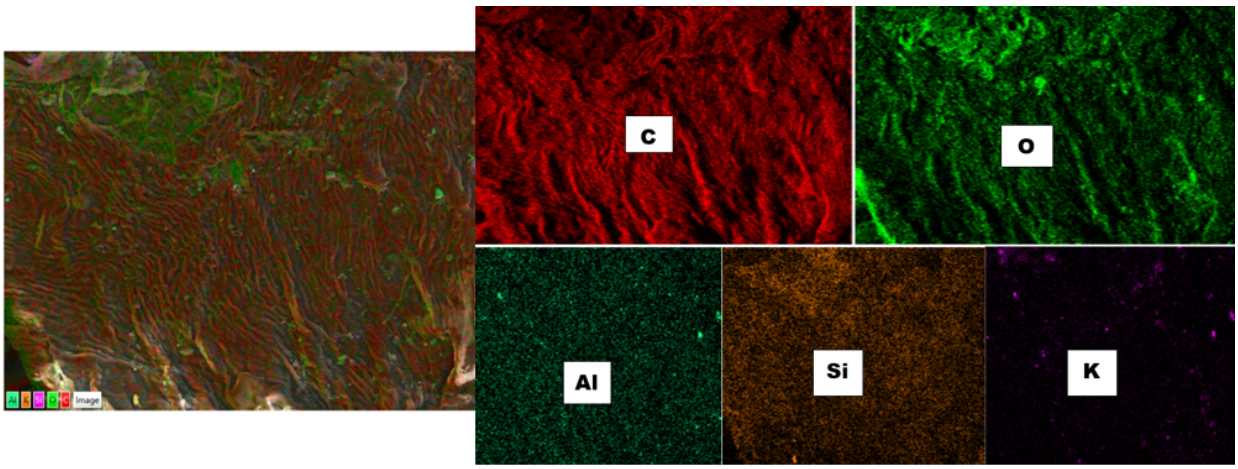

Figure 4. EDX image illustrating the main elements constituent of ABPC

Table 1. FTIR Analysis, chemical bonds

Waves numbers (cm^{-1})	3655	2956 2914	2836 2877	2173 2034	1739	1453 1372	1294 1155	969 836
Bonds	O-H	C-H	C-H	C≡C C=N	C=O	C=C C-C O-H	P-O-C P=O P=OOH	C-H

Table 2. Atomic percentages of chemical elements in ABPC

Element	**C**	**O**	**K**	**Al**	**Mg**	**Si**	**P**	**Ca**	**S**	**Cl**
% atomic	77.83	20.86	0.52	0.20	0.18	0.13	0.11	0.12	0.03	0.02

3.7 Adsorption study

3.7.1 Influences of initial solution concentrations

Figure 5.a shows the percentage of MB adsorption per unit mass of ABPC as a function of time, at different initial MB concentrations ($20\,mg\cdot L^{-1}$, $30\,mg\cdot L^{-1}$, $40\,mg\cdot L^{-1}$ and $50\,mg\cdot L^{-1}$). It can be seen that the removal of the MB dye is approximately 98% in about 30 minutes. The maximum rate of removal is highly dependent on the initial concentrations of the solutions. The removal time is shorter for solutions with low initial concentrations than for solutions with high concentrations.

3.7.2 Mass influences of activated carbon

Figure 5.b shows the percentage of MB adsorption per unit mass of ABPC as a function of time at different masses (0.1 g, 0.2 g, and 0.3 g). The maximum percentage of MB adsorbed is reached at a short time as the mass of ABPC increases. The greater the mass of activated carbon used, the faster the adsorption reaction of MB onto ABPC. The number of adsorption sites increases with the mass of the adsorbent. Access to adsorption sites by dye molecules promotes rapid dye removal at shorter times.

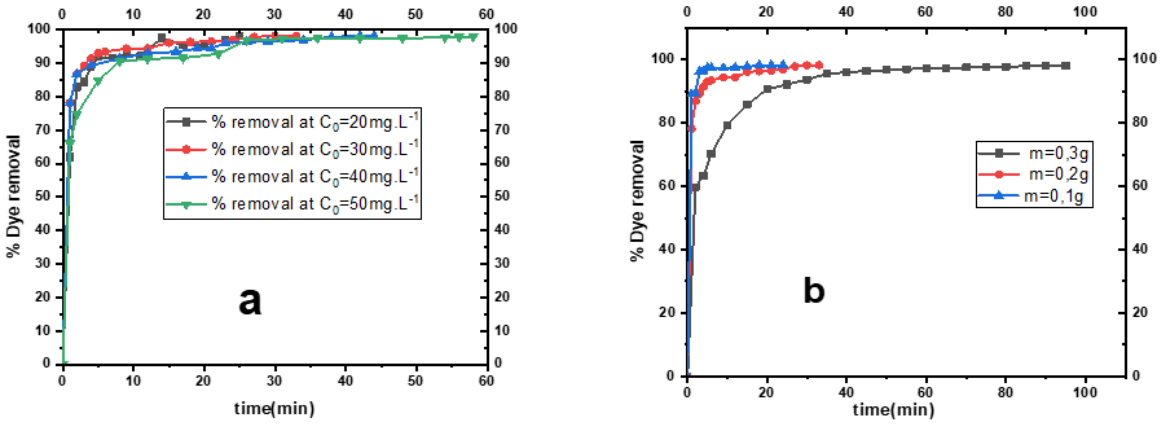

Figure 5. Influence of initial concentration (a) and influence of mass (b) on the percentage of MB elimination versus time

3.7.3 Intra-particle diffusion and isotherms

3.7.3.1 Adsorption isotherms

Adsorption isotherms relate, at a given temperature, the quantities of adsorbate molecules to the quantities of adsorbent at equilibrium. They allow for the analysis of experimental data and facilitate the description of pollutant adsorption. The Langmuir and Freundlich models were applied for the analysis of experimental data of the adsorbent-pollutant system. The experimental results are illustrated in **Figure 6** and **Table 4.** The Langmuir separation factor (R_L) calculated from **Eqn. 9** is respectively 0.022, 0.015, 0.011, 0.009 for BM solutions with initial concentrations of 20 $mg \cdot L^{-1}$, 30 $mg \cdot L^{-1}$, 40 $mg \cdot L^{-1}$, and 50 $mg \cdot L^{-1}$ and the linear correlation coefficient (R^2) is 0.95. Note that the Langmuir separation factor R_L is such that $0 < R_L < 1$. Therefore, the adsorption process of MB on ABPC is favorable. This implies that the adsorption of MB on the adsorption surfaces occurs in a monolayer with a reduction of interactions between molecules (Baari *et al.*, 2025; Din *et al.*, 2024).

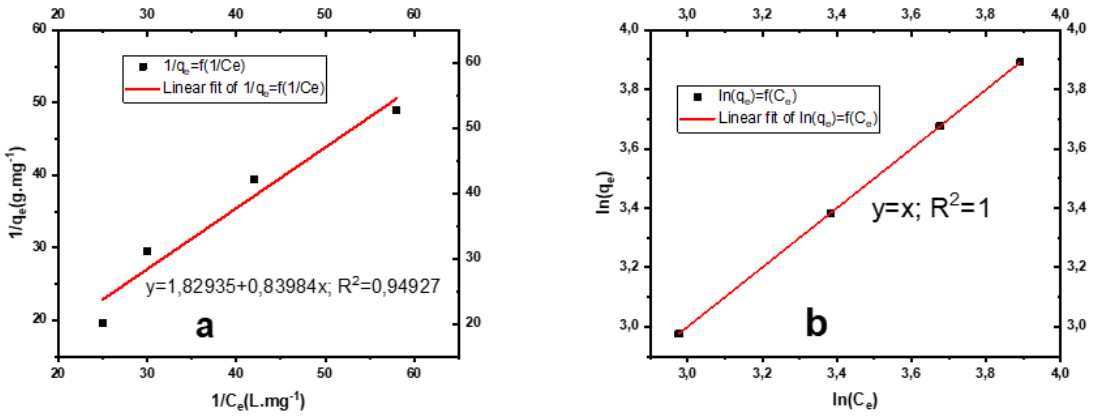

Figure 6. Langmuir isotherm (a) and Freundlich isotherm (b)

The graph of $\ln(q_e)$ versus $\ln(C_e)$ is linear, with a correlation coefficient R^2 equals 1. The constants K_f and $\frac{1}{n}$ are both equal to 1. The correlation coefficient of the Freundlich model is significantly higher than that of the Langmuir model. Therefore, the Freundlich isotherm model appears better suited to the adsorption of MB onto the ABPC. This suggests that MB adsorption

occurs through the formation of a multilayer structure on a non-homogeneous surface, with interactions between the molecules constituting the layers.

3.7.3.2 Adsorption kinetics

Pseudo-first-order and pseudo-second-order adsorption kinetics were applied to analyze the sorption of methylene blue onto activated carbon. Pseudo-first-order adsorption kinetics implies that the reaction rate is proportional to the methylene blue concentration and controlled by surface interactions; furthermore, the adsorption reaction rate increases with the number of available adsorption sites. However, the pseudo-second-order kinetic model posits a chemical adsorption process with distinct steps. The graphs representing the first-order and second-order models are shwon in **Figure 7**. The results of the calculations of the rate constants, the quantities of MB adsorbed per unit mass of coal at equilibrium and the experimental values as well as the intraparticle diffusion parameters are presented in **Table 3.**

The experimental values of the amount of BM adsorbed per unit mass of carbon at equilibrium (19.61, 29.47, 39.45, 48.95 $mg \cdot L^{-1}$) show a large discrepancy with the amounts of MB adsorbed calculated using pseudo-first-order kinetics (3.76, 3.83, 6.80, 12.00 $mg \cdot g^{-1}$). This discrepancy implies that there is no correlation between the experimental data and the calculation according to the first-order kinetic model. Consequently, it is deduced that the adsorption of the MB dye by ABPC does not follow the pseudo-first-order kinetic model. The pseudo-first-order kinetic model of adsorption is not suitable for describing the adsorption mechanism of methylene blue on ABPC. Regarding the second-order kinetic model, it should be noted that the results of the Calculations of the quantities of BM adsorbed per unit mass of coal at equilibrium (19.85; 29.67; 39.77; 49.65 $mg \cdot g^{-1}$) are approximately equal to the experimental data (19.61, 29.47; 39.45; 48.95 $mg \cdot g^{-1}$). The plot of the representative curves $\frac{t}{q_t}$ versus t is linear, and the value of correlation coefficient R^2 (0.99) is close to 1, regardless of the initial concentrations of the solutions. The second-order adsorption kinetics model better describes the adsorption of MB on the ABPC, as it appears to fit the experimental data better. Consequently, the removal of MB by ABPC is potentially chemisorption-related; this involves not only valence forces, or electron exchange, but also interactions between the adsorbate molecules and the adsorbent surface (Abdelhafez *et al*., 2025; Luo *et al*., 2025). It is these interactions that potentially facilitated the removal of the MB dye.

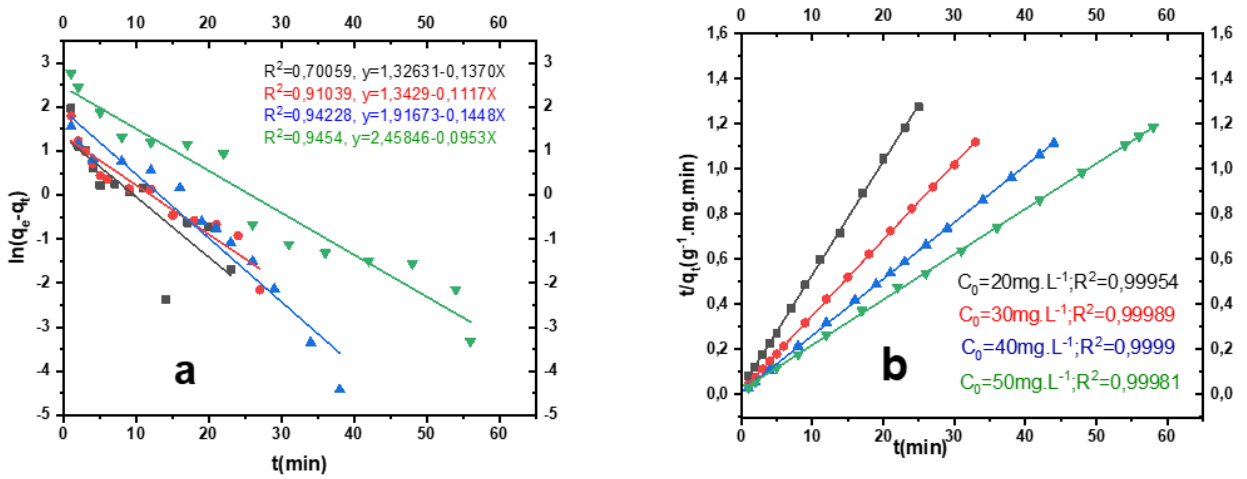

Figure 7. Pseudo-First-order kinetic model (a) and Pseudo-second-order kinetic model (b)

Table 3. Pseudo-first order, pseudo-second order and intra-particle diffusion kinetics models

C_0 ($g \cdot mg^{-1}$)	$q_{e,exp}$ $mg \cdot g^{-1}$	Pseudo-first order			Pseudo-second order			Intra-particle diffusion		
		k_1 min^{-1}	q_e $mg \cdot g^{-1}$	R^2	k_2 $g \cdot mg^{-1} \cdot min^{-1}$	q_e $mg \cdot g^{-1}$	R^2	k_d $mg \cdot g^{-1} \cdot min^{-\frac{1}{2}}$	C $mg \cdot g^{-1}$	R^2
20	19.61	0.13	3.76	0.70	0.09	19.85	0.99	1.25	14.26	0.63
30	29.47	0.11	3.83	0.91	0.01	29.67	0.99	1.16	24.36	0.72
40	39.45	0.14	6.79	0.94	0.06	39.77	0.99	0.99	34.47	0.90
50	48.95	0.09	12.00	0.94	0.02	49.65	0.99	3.38	32.72	0.81

Table 4. Langmuir and Freundlich isotherm parameters

Adsorption isotherm	Langmuir isotherm			Freundlich isotherm		
Constants	q_m $(mg \cdot g^{-1})$	K_L $(mg \cdot L^{-1})$	R^2	K_F $(mg \cdot g^{-1})$	n	R^2
	0.54	2.17	0.95	1	1	1

3.7.3.3 Intra-particle diffusion

The study of dye sorption can be explained by the intraparticle diffusion model. The curves representing the amount of dye adsorbed per unit mass of adsorbent (q_t) versus the square root of time ($t^{\frac{1}{2}}$) are shown in **Figure 8.a**. Characteristic parameters such as the diffusion rate constant (k_d), the correlation coefficient (R^2), and the diffusion constant (C) have been calculated and are illustrated in **Table 3.** The diffusion constant being positive implies that the diffusion process to the sites happens quickly and adsorption is rapid (Bassareh *et al.*, 2023; Wang & Guo, 2022).

Figure 8.b illustrates the amount of MB adsorbed per unit mass of ABPC versus time (t), at different initial MB concentrations ($20\,mg \cdot L^{-1}$, $30\,mg \cdot L^{-1}$, $40\,mg \cdot L^{-1}$, $50\,mg \cdot L^{-1}$). The resulting curves show three phases, indicating that MB adsorption occurs in three phases. In the first phase,

adsorption is rapid, becomes slow in the second phase, and then approaches equilibrium in the third phase. Since free adsorption sites are available in the first phase, the molecules migrate from the dye to the surface of the carbon and then into the internal pores where they are adsorbed.

The number of adsorption sites decreases as the process continues; this would explain the slowness of adsorption until equilibrium is reached. At the initial concentration of $40\,mg\cdot L^{-1}$, the diffusion coefficient $k_d(0.99\,mg\cdot g^{-1}\cdot min^{-\frac{1}{2}})$ is smaller, but the linear correlation coefficient $R^2(0.90)$ is higher, and the corresponding diffusion constant C $(34.47\,mg\cdot g^{-1})$ is greater. Therefore, the diffusion of MB dye particles into the pores of activated carbon under these conditions is not only slow, but the maximum amount of MB adsorbed per unit mass of carbon is also greater. Thus, the best adsorption condition for MB on carbon is when the initial concentration of methylene blue is close to $40\,mg\cdot L^{-1}$.

The adsorption of MB onto ABPC was carried out under conditions where the initial pH of the MB (cationic dye) solutions was acidic, but exceeded the pH at the point of zero charge $(pH_{ZPC}=5{,}16)$ of ABPC. Thus, the surface of the carbon is predominantly negatively charged, and adsorption is controlled by electrostatic interactions on the one hand. Electron interactions π-π due to the presence of aromatic rings in both the structure of the dye and the activated carbon derived from bean pods (cellulose, hemicellulose, lignin) are favorable to adsorption on the other hand (Bortoluz *et al.*, 2020).

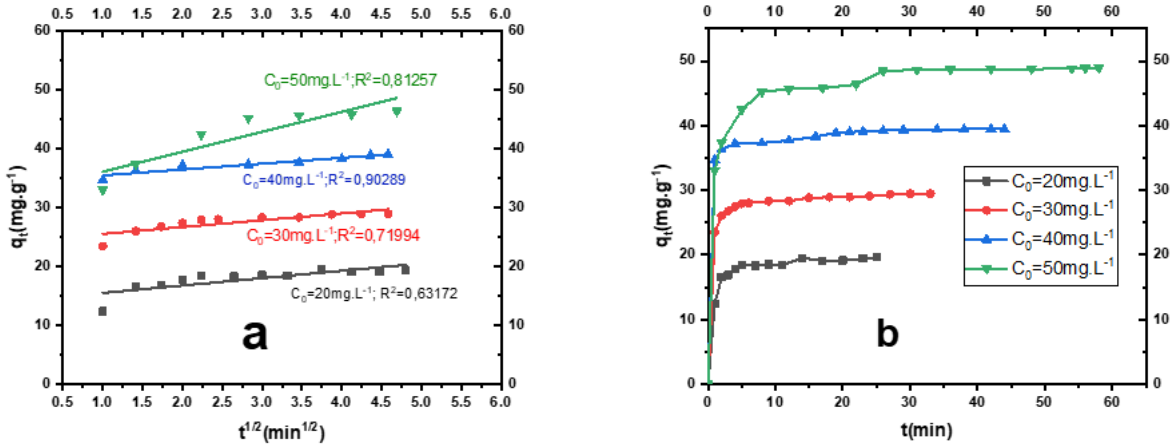

Figure 8. Intra-particle diffusion (a) and amount of MB adsorbed per gram of ABPC versus time at different initial concentrations (b)

Conclusion

The production of activated carbon from bean pods by chemical activation with 50% phosphoric acid was successfully carried out. The activation rate exceeding 50% implies that the activated carbon would tend to develop meso- and macropores during pyrolysis at 400°C. X-ray diffraction analysis and the low ash content (5.4%) indicate that the activated carbon prepared by chemical activation with phosphoric acid is an amorphous solid. Infrared analysis revealed the presence of functional groups characteristic of carboxylic acids, alkenes, lactones, carbonyls, amines, amides, and phosphorus compounds. Scanning electron microscopy (SEM) coupled with energy-dispersive X-ray

spectroscopy (EDX) illustrated the heterogeneous pore distribution and the elemental chemical composition of the carbons. Indeed, the predominant atoms constituting activated carbon are carbon (77.83%) and oxygen (20.86%), followed by small amounts of magnesium, potassium, and phosphorus. Based on the physicochemical characterization results, the activated carbon obtained possesses good characteristics, and its application for removing pollutants from wastewater is feasible. Energy-dispersive X-ray (EDX) analysis of the activated carbon highlights the presence of carbon and oxygen. The characterization and experimental results reveal that the activated carbon from bean pods is amorphous, with a MB removal rate exceeding 98%. It is therefore a potential alternative adsorbent for wastewater treatment. The pseudo-second-order kinetic model best describes the adsorption of methylene blue by the carbon. The best conditions for intra-particle diffusion are those in which the initial concentration of the solution is close to 40 $mg \cdot L^{-1}$.

Acknowledgments: The authors are grateful to the directors and all the technicians of laboratories « Laboratoire de Grestion, Traitement et Valorisation des Déchets (GTVD), Laboratoire d'Hydrologie Appliquée et Environnement (LHAE), Université de Lomé, Togo »

Disclosure statement: The authors declare no conflicts of interest that could have influenced the publication of this paper.

Compliance with Ethical Standards: This article does not contain any studies involving human or animal subjects.

References

Abdelhafez, T. F., Radwan, E. K., Sayed, G. H., El Khatib, E. M., Nasr, M. F., & El Gabry, L. K. (2025). Removal of acid and basic dyes from textile wastewater using modified acrylic fibres waste as an efficient adsorbent. *Scientific Reports*, *15*(1), 23825. https://doi.org/10.1038/s41598-025-07134-y

Akartasse N., Azzaoui K., Mejdoubi E., Hammouti B., Elansari L.L., Abou-salama M., Aaddouz M., Sabbahi R., Rhazi L. and Siaj M. (2022), Environmental-Friendly Adsorbent Composite Based on Hydroxyapatite/Hydroxypropyl Methyl-Cellulose for Removal of Cationic Dyes from an Aqueous Solution, *Polymers*, 14(11), 2147; https://doi.org/10.3390/polym14112147

Al Lafi, A. G., & Khuder, A. (2025). Removal of Cr(VI) from aqueous solutions by activated carbon and its composite with P2W17O61: A spectroscopic study to reveal adsorption mechanism. *Heliyon*, *11*(2), e41862. https://doi.org/10.1016/j.heliyon.2025.e41862

Al-Asadi, S. T., Mussa, Z. H., Al-Qaim, F. F., Kamyab, H., Al-Saedi, H. F. S., Deyab, I. F., & Kadhim, N. J. (2025). A comprehensive review of methylene blue dye adsorption on activated carbon from edible fruit seeds: A case study on kinetics and adsorption models. *Carbon Trends*, *20*, 100507. https://doi.org/10.1016/j.cartre.2025.100507

Aljeboree, A. M., Abdulrazzak, F. H., Saleh, Z. M., Abbas, H. A., & Alkaim, A. F. (2024). Eco-Friendly Adsorption of Cationic (Methylene Blue) and Anionic (Congo Red) Dyes from Aqueous Solutions Using Sawdust. *RAiSE-2023*, 213. https://doi.org/10.3390/engproc2023059213

Aljeboree, A. M., Alshirifi, A. N., & Alkaim, A. F. (2014). Kinetics and equilibrium study for the adsorption of textile dyes on coconut shell activated carbon. *Arabian Journal of Chemistry*, *10*, S3381–S3393. https://doi.org/10.1016/j.arabjc.2014.01.020

Alkhawaja, E. S., & Abdul-Hameed, H. M. (2025). Novel Synthesis and Characterization of Nano-Activated Carbon Derived from Agricultural Orange Peel Waste. *International Journal of Design & Nature and Ecodynamics*, *20*(1), 31–41. https://doi.org/10.18280/ijdne.200104

Allahkarami, E., Dehghan Monfared, A., Silva, L. F. O., & Dotto, G. L. (2023). Toward a mechanistic understanding of adsorption behavior of phenol onto a novel activated carbon composite. *Scientific Reports*, *13*(1). https://doi.org/10.1038/s41598-023-27507-5

Alouiz, I., Aqil, M., Chari, A., Dahbi, M., Amarouch, M. Y., & Mazouzi, D. (2025). Influence of phosphorus activation and carbonization temperature on the electrochemical performance of hard carbon made from olive pomace as an anode for sodium-ion batteries. *RSC Advances*, *15*(25), 19546–19560. https://doi.org/10.1039/d5ra02547h

Armand, A. E., Augustin, Y. Y., Urbain, K. Y., & Albert, T. (2020). Optimisation de la préparation de charbons activés à base d'épis de maïs et caractérisation physico-chimique. *International Journal of Innovation and Applied Studies, © 2020 Innovative Space of Scientific Research Journals*, *29*(4), 1161–1171. http://www.ijias.issr-journals.org/

Asuquo, E., Martin, A., Nzerem, P., Siperstein, F., & Fan, X. (2017). Adsorption of Cd(II) and Pb(II) ions from aqueous solutions using mesoporous activated carbon adsorbent: Equilibrium, kinetics and characterisation studies. *Journal of Environmental Chemical Engineering*, *5*(1), 679–698. https://doi.org/10.1016/j.jece.2016.12.043

Atheba, P., Gbassi, G. K., Dongui, B., Bamba, D., Yolou, S., & Trokourey, A. (2014). Études de la porosité, de la surface spécifique et des fonctions de surface de charbons actifs préparés après carbonisation artisanale des coques de noix de coco. *: https://www.researchgate.net/publication/266676067*, *8*(34). : https://www.researchgate.net/publication/266676067

Baari, M. J., Rudi, L., & Harimu, L. (2025). Adsorption isotherms, thermodynamics, and kinetics of activated carbon as adsorbent to water pollutants: A review. *Chimica Techno Acta*, *12*(2). https://doi.org/10.15826/chimtech.2025.12.2.14

Balogoun, C., Bawa, M., Osseni, S., & Aina, M. (2015). Préparation des charbons actifs par voie chimique à l'acide phosphorique à base de coque de noix de coco. *International Journal of Biological and Chemical Sciences*, *9*(1), 563. https://doi.org/10.4314/ijbcs.v9i1.48

Bassareh, H., Karamzadeh, M., & Movahedirad, S. (2023). Synthesis and characterization of cost-effective and high-efficiency biochar for the adsorption of Pb2+ from wastewater. *Scientific Reports*, *13*(1). https://doi.org/10.1038/s41598-023-42918-0

Bortoluz, J., Ferrarini, F., Bonetto, L. R., Da Silva Crespo, J., & Giovanela, M. (2020). Use of low-cost natural waste from the furniture industry for the removal of methylene blue by adsorption: Isotherms, kinetics and thermodynamics. *Cellulose*, *27*(11), 6445–6466. https://doi.org/10.1007/s10570-020-03254-y

Brou Guillaume, K., Serpokrylov, N. S., Smolyanichenko, A. S., Cheblakova, E. G., Gorina, V. A., & Yoboué, D. V. (2019). Physico-chemical characteristics of the char from cashew nuts shells and activated carbons obtained from it. *Environnement, Ingénierie & Développement*, *N°82-décembre 2019*, 7728. https://doi.org/10.4267/dechets-sciences-techniques.4164

Collins Ngoe, E., Bopda, A., Tchuifon Donald, T., & George Ndifor-Angwafor, N. (2018). Application of response surface methodology for the removal of 4-nitroaniline in aqueous solution using activated carbon prepared from peanut shells and avocado seed. *International Journal of Research Publications*, *09*. https://doi.org/10.47119/IJRP1009172018292

Diallo, A. D., Bangoura, M., & Sakho, A. M. (2022). Essai d'épuration d'eaux usées par double filtration sur charbon actif en poudre préparé à partir des coques d'arachides. *Rev. Ivoir. Sci. Technol.*, *40*, 101–110. http://www.revist.ci

Din, H., Kiran, M., Haq, F., Osman, A. I., Khan, I. A., Aziz, T., Khan, A., & Jilani, S. (2024). Synergizing date palm seeds-derived oxidized activated carbon: Sustainable innovation for enhanced water retention, efficient wastewater treatment, and synthetic dye removal. *Chemical Engineering Research and Design*, *204*, 212–227. https://doi.org/10.1016/j.cherd.2024.02.040

Dunston, A. K., Lenin, A., Kumar, P., Veerappan, G., Seenivasan, G. B., Thakur, A., & Sivakumar, A. (2025). Sequestration of lead ion pollutants onto copper doped activated carbon nanoparticles derived from

Phaseolus vulgaris L. (bean husk). *Matéria (Rio de Janeiro)*, *30*. https://doi.org/10.1590/1517-7076-rmat-2024-0689

Faouzou, O.-A., Amenuvevega, D. A., Ibrahim, T., Samadou, S., Tomkouani, K., Seyf-Laye, A.-S. M., & Moctar, B. L. (2024). Synthesis of Activated Carbon from Cassava Peeling and Its Applications for Removal of Methylene Blue. *American Journal of Physical Chemistry*, *13*(1), 9–16. https://doi.org/10.11648/j.ajpc.20241301.12

Farma, R. (2019). Physical Properties Analysis of Activated Carbon from Oil Palm Empty Fruit Bunch Fiber on Methylene Blue Adsorption. *Journal of Technomaterials Physics*, *1*(1), 67–73. https://doi.org/10.32734/jotp.v1i1.824

Fathy, N. A., Sayed Ahmed, S. A., & Abo El-enin, R. M. M. (2012). Effect of Activation Temperature on Textural and Adsorptive Properties for Activated Carbon Derived from Local Reed Biomass: Removal of p-Nitrophenol. *Environmental Research, Engineering and Management*, *59*(1), 10–22. https://doi.org/10.5755/j01.erem.59.1.961

Fitri Faradilla, R. H., Lucia, L., & Hakovirta, M. (2021). Hydrothermal carbonization of soybean hulls for the generation of hydrochar: A promising valorization pathway for low value biomass. *Environmental Nanotechnology, Monitoring & Management*, *16*, 100571. https://doi.org/10.1016/j.enmm.2021.100571

Hazourli, S., & Ziati, M. C. (2007). Valorisation d'un résidu naturel ligno-cellulosique en charbon actif - exemple des noyaux de dattes-. *Revue des Energies renouvelables ICRESD-07 Clemcen*, 187–192.

Ismail, B. M., Zayed, A. M., Roshdy, M. A., Rafea, M. A., & Mohamed, F. M. (2025). Statistical modeling of mutagenic azo dye adsorption on bagasse activated carbon. *Scientific Reports*, *15*(1). https://doi.org/10.1038/s41598-025-04240-9

Kaga, T. T., Segbeaya, K. N., Pallier, V., & Feuillade, G. (2024). Synthesis and Characterization of Activated Carbons from Avocado Kernel; Application to Phenol Removal. *American Journal of Materials Science and Engineering*, *12*(1), 1–12. https://doi.org/10.12691/ajmse-12-1-1

Kanawade, S. M., & Gaikwad, R. W. (2011). Adsorption of heavy metals by activated carbon synthesized from solid wastes. *International Journal of Chemical Engineering and Applications*, *2*(3), 207–211. https://doi.org/10.7763/IJCEA.2011.V2.104

Khadiran, T., Hussein, M. Z., Zainal, Z., & Rusli, R. (2014). Textural and Chemical Properties of Activated Carbon Prepared from Tropical Peat Soil by Chemical Activation Method. *BioResources*, *10*(1), 986–1007. https://doi.org/10.15376/biores.10.1.986-1007

Kifuani Kia Mayeko, A., Noki Vesituluta, P., Ndelo Di Phanzu, J., Mukana Wa Muanda, D., Ekoko Bakambo, G., Ilinga Lopaka, B., & Mukinayi Mulangala, J. (2012). Adsorption de la quinine bichlorhydrate sur un charbon actif peu coûteux à base de la Bagasse de canne à sucre imprégnée de l'acide phosphorique. *International Journal of Biological and Chemical Sciences*, *6*(3), 1337–1359. https://doi.org/10.4314/ijbcs.v6i3.36

Kumaravel, S., Geetha, M., Niyitanga, T., Kumar, D. S., Al-Ansari, M. M., Mythili, R., Suganthi, S., Guganathan, L., Murugan, A., & Ragupathy, S. (2024). Preparation and characterization of activated carbon from corn cob by chemical activation and their adsorption of brilliant green dye from wastewater. *Process Safety and Environmental Protection*, *188*, 1338–1345. https://doi.org/10.1016/j.psep.2024.05.127

Luo, X., Wang, H., Ren, X., Liu, G., Luo, H., Zheng, Z., & Wu, F. (2025). Effective adsorptive removal of heavy metal anion Cr(VI) and dye cation methylene blue by the novel 2D material TiVCTx MXene. *Journal of Alloys and Compounds*, *1010*, 177409. https://doi.org/10.1016/j.jallcom.2024.177409

Lv, Z., Wang, Z., Wang, H., Li, J., & Li, K. (2024). Adsorption of cationic/anionic dyes and endocrine disruptors by yeast/cyclodextrin polymer composites. *RSC Advances*, *14*(10), 6627–6641. https://doi.org/10.1039/D3RA07682B

Maazou, S. D. B., Hima, H. I., Malam Alma, M. M., Adamou, Z., & Natatou, I. (2018). Elimination du chrome par du charbon actif élaboré et caractérisé à partir de la coque du noyau de *Balanites*

aegyptiaca. *International Journal of Biological and Chemical Sciences*, *11*(6), 3050. https://doi.org/10.4314/ijbcs.v11i6.39

Mahmoud, M. R., Mahgoub, S. M., Abdelazeem, R., Abdelsatar, M. M., Allam, A. A., Alfassam, H. E., Radalla, A. M., & Mahmoud, R. (2025). RP-HPLC method development and validation for the quantification of prednisolone and salbutamol with their simultaneous removal from water using modified clay–activated carbon adsorbents. *RSC Advances*, *15*(11), 8675–8695. https://doi.org/10.1039/d5ra00324e

Mamane, O. S., Boukari, M. S. D., & Chaibou, A. R. (2018). *Valorisation de coques de noix de Balanitesaegyptiaca(L.)Del.et élimination du Chrome en solution*. *14*(3), 167–181. http://www.afriquescience.net

Ojstršek, A., & Gorgieva, S. (2024). Cellulose Nanofibrils-Reinforced Pectin Membranes for the Adsorption of Cationic Dyes from a Model Solution. *Polymers*, *16*(6), 724. https://doi.org/10.3390/polym16060724

Ojstršek, A., Vouk, P., & Fakin, D. (2022). Adsorption of Pollutants from Colored Wastewaters after Natural Wool Dyeing. *Materials*, *15*(4), 1488. https://doi.org/10.3390/ma15041488

Olorundare, O. F., Msagati, T. A. M., Krause, R. W. M., Okonkwo, J. O., & Mamba, B. B. (2014). Activated Carbon from Lignocellulosic Waste Residues: Effect of Activating Agent on Porosity Characteristics and Use as Adsorbents for Organic Species. *Water, Air, & Soil Pollution*, *225*(3), 1876. https://doi.org/10.1007/s11270-014-1876-2

Ouedrhiri, M., Jaaouan, K., Mohtadi, F. E., Benismail, C., & Begdouri, A. A. (2018). Charbons actifs à partir des coques d'olives (Picholine marocaine): Préparation, caractérisation et évaluation de leur capacité de dépollution des margines. *Rev. Mar. Sci. Agron. Vét*, *6*(3), 362–373.

N'diaye A.D., Hammouti B., Nandiyanto A. B. D., Al Husaeni D. F. (2022), A review of biomaterial as an adsorbent: From the bibliometric literature review, the definition of dyes and adsorbent, the adsorption phenomena and isotherm models, factors affecting the adsorption process, to the use of Typha species waste as a low-cost adsorbent, *Communications in Science and Technology*, 7 No.1, 140-153, https://dx.doi.org/10.21924/cst

Raheel, F., Rafay, A., Bibi, B., Ahmad, S., Ali, Z., Saleem, M., Butt, M. S., Rehman, A. U., & Irfan, M. (2024). Synthesis and Characterization of Activated Carbon and Its Application for Wastewater Treatment. *CEMP 2023*, 4. https://doi.org/10.3390/materproc2024017004

Salama, Reda. S., Gouda, M. S., Aboud, M. F. A., Alshorifi, F. T., El-Hallag, A. A., & Badawi, A. K. (2024). Synthesis and characterization of magnesium ferrite-activated carbon composites derived from orange peels for enhanced supercapacitor performance. *Scientific Reports*, *14*(1). https://doi.org/10.1038/s41598-024-54942-9

Saleem, J., Moghal, Z. K. B., Tahir, F., Al-Ansari, T., & McKay, G. (2025). Environmental Impacts and Adsorption Isotherms of Coconut Shell Activated Carbon: Effect of Acid Activation, Water, and Fuel. *C*, *11*(1), 22. https://doi.org/10.3390/c11010022

Saleem, M. (2024). Sustainable production of activated carbon from indigenous Acacia etbaica tree branches employing microwave induced and low temperature activation. *Heliyon*, *10*(2), e24113. https://doi.org/10.1016/j.heliyon.2024.e24113

Sanni, S., Tchakala, I., Kodom, T., Karamoko, B. A., Bawa, L. M., & Holade, Y. (2025). Activated Carbons Derived from Brewing Cereal Residues and Pineapple Peelings for Removal of Acid Orange 7 (AO7) Dye. *Molecules*, *30*(4), 881. https://doi.org/10.3390/molecules30040881

Shamsuddin, M. S., Yusoff, N. R. N., & Sulaiman, M. A. (2016). Synthesis and Characterization of Activated Carbon Produced from Kenaf Core Fiber Using H3PO4 Activation. *Procedia Chemistry*, *19*, 558–565. https://doi.org/10.1016/j.proche.2016.03.053

Sudarsan, S., Murugesan, G., Varadavenkatesan, T., Vinayagam, R., & Selvaraj, R. (2025). Efficient adsorptive removal of Congo Red dye using activated carbon derived from Spathodea campanulata flowers. *Scientific Reports*, *15*(1). https://doi.org/10.1038/s41598-025-86032-9

Suyoga Wiguna, A. A. G., Mardana, I. B. P., & Artawan, P. (2024). Synthesis and characterization of activated carbon prepared from rice husk by physics-chemical activation. *Indonesian Physical Review*, *7*(2), 281–290. https://doi.org/10.29303/ipr.v7i2.311

Tchakala, I., Bawa, L., Djaneye-Boundjou, G., Doni, K., & Nambo, P. (2012). Optimisation du procédé de préparation des Charbons Actifs par voie chimique (H_3PO_4) à partir des tourteaux de Karité et des tourteaux de Coton. *International Journal of Biological and Chemical Sciences*, *6*(1), 461–478. https://doi.org/10.4314/ijbcs.v6i1.42

Touzani, I., El Machrafi I., Harboul K., Boudouch O., Alouiz I., Hammani K., Flouchi R., Fikri-Benbrahim K. (2024). Evaluation of Activated Carbons Prepared from Bioprecursors for the Removal of Cadmium and Chromium(VI). *Applied and Environmental Soil Science*, 2024, 1–11. https://doi.org/10.1155/2024/8663114

Usman, A. S., Ibrahim, M. B., Bishir, U. (2025). Adsorption of Dyes from Synthetic Wastewater using Doum Palm Activated Carbon. *S. Afr. J. Chem.*, *79*, 10–17. https://doi.org/10.17159/0379-4350/2025/v79a02

Wang J., Guo X. (2022). Rethinking of the intraparticle diffusion adsorption kinetics model: Interpretation, solving methods and applications. *Chemosphere*, 309, 136732. https://doi.org/10.1016/j.chemosphere.2022.136732

Yunusa, Umar, Yunusa, U., Usman, B., Department of Pure and Industrial Chemistry, Bayero University, P.M.B.3011, BUK, Kano-Nigeria, Bashir Ibrahim, M., & Department of Pure and Industrial Chemistry, Bayero University, P.M.B.3011, BUK, Kano-Nigeria. (2020). Adsorptive Removal of Basic Dyes and Hexavalent Chromium from Synthetic Industrial Effluent: Adsorbent Screening, Kinetic and Thermodynamic Studies. *International Journal of Engineering and Manufacturing*, *10*(4), 54–74. https://doi.org/10.5815/ijem.2020.04.05

Zayed, A. M., Metwally, B. S., Masoud, M. A., Mubarak, M. F., Shendy, H., Petrounias, P., & Abdel Wahed, M. S. M. (2023). Facile synthesis of eco-friendly activated carbon from leaves of sugar beet waste as a superior nonconventional adsorbent for anionic and cationic dyes from aqueous solutions. *Arabian Journal of Chemistry*, *16*(8), 104900. https://doi.org/10.1016/j.arabjc.2023.104900

Zięzio, M., Charmas, B., Jedynak, K., Hawryluk, M., & Kucio, K. (2020). Preparation and characterization of activated carbons obtained from the waste materials impregnated with phosphoric acid(V). *Applied Nanoscience*, *10*(12), 4703–4716. https://doi.org/10.1007/s13204-020-01419-6